Received: 26 July 2020 | Revised: 20 November 2020 | Accepted: 12 March 2021

IET Electrical Systems in Transportation

DOI: 10.1049/els2.12024

The Institution of Engineering and Technology WILEY

ORIGINAL RESEARCH PAPER

Development of steady arm damper for electrified railway overhead contact line with double pantographs based on numerical and experimental analysis

Wenping Chu[1] | **Yang Song**[2] | **Fuchuan Duan**[1] | **Zhigang Liu**[1]

[1]National Rail Transit Electrification and Automation Engineering Technique Research Centre, Southwest Jiaotong University, Chengdu, China

[2]Department of Structural Engineering, Norwegian University of Science and Technology, Trondheim, Norway

Correspondence

Yang Song, Department of Structural Engineering, Norwegian University of Science and Technology, Trondheim, 7491 Norway.
Email: y.song_ac@hotmail.com

Funding information

National Natural Science Foundation of China-Guangdong Joint Fund, Grant/Award Number: U1734202; U51977182; the Funding of Chengdu Guojia Electrical Engineering Co. Ltd, Grant/Award Number: NEEC-2019-B09

Abstract

To improve the carrying capacity, double pantographs are normally used to collect the electric current from the catenary. The mechanical wave excited by the leading pantograph affects the contact of the trailing pantograph and the contact wire, which usually deteriorates the current collection quality. To address this issue, a steady arm damper is developed in this work to reduce the wave intensity caused by the leading pantograph. The catenary is modelled by Absolute Nodal Coordinate Formulation. The numerical simulations indicate that the steady arm damper with certain values reduces the contact force variation of the trailing pantograph. But overlarge damping may behave as a hard spot and aggravates the interaction performance. The acceptable steady arm damping should be lower than 300 Ns/m. The optimal value of the steady arm damping coefficient varies with the train speed. The realistic damping ratio should be determined based on the operating speed of a railway line. Based on the simulation results, several realistic steady arm dampers are developed, which are placed between the cantilever and the end of the steady arm. An experimental test is conducted to investigate the effect of the steady arm damper on the reduction of vibration caused by the dropping sinker. The experimental results demonstrate that the steady arm damper can reduce the mechanical wave amplitude and eliminate its effect on the trailing pantograph.

1 | INTRODUCTION

The last two decades have witnessed the rapid expansion of high-speed network mileage around the world. The demand for higher carrying capacity and faster speed poses new technical challenges. One of them is to ensure the good current collection quality of the pantograph-catenary system. To increase the carrying capacity of the high-speed train, the effective measure is to connect two electric multiple units (EMUs). So the electric train is equipped with double pantographs to collect the current from the catenary, as shown in Figure 1. Two pantographs are interacting with the catenary simultaneously. The mechanical wave excited by the leading pantograph propagates towards the trailing pantograph and disturbs its contact with the contact wire. In reality, the trailing pantograph often has unsatisfactory current collection quality. Arcing and contact loss are frequently observed from the monitoring of the trailing pantograph. In China, Europe and Japan, the double-pantograph operation has been widely adopted in high-speed networks to ensure the sufficient current collection capacity of the electric trains.

The pantograph-catenary interaction performance has attracted ever-increasing attention from both the academic community and the industry, as it is of great importance to enable safe and stable operation of electric railway without traffic disorders. Various types of mathematical models have been proposed based on the mode superposition method [1], explicit formulas [2, 3], finite element method [4], absolute nodal coordinate formulation [5] as well as finite difference method [6]. To understand the effect of geometrical and material properties on interaction performance, the sensitivity analysis was performed by Zhang et al. [7]. The optimisation

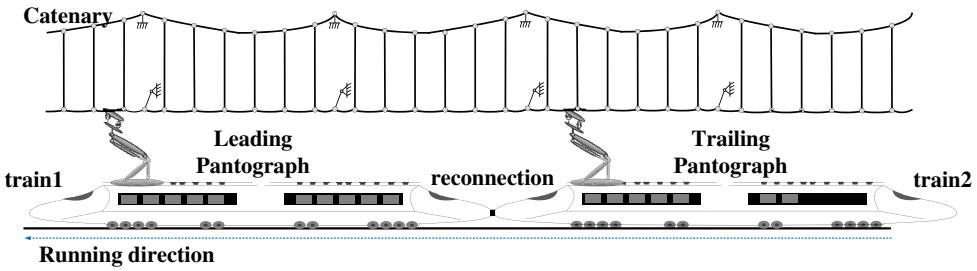

FIGURE 1 Schematics of double pantographs-catenary system

strategy for better current collection quality was proposed [8]. Contact loss, which is the primary source of arcing and sparking between the pantograph collector and the contact wire was numerically simulated and investigated [9]. The arcing detection approach based on support vector machines was developed by Barmada et al. [10]. The study on the effect of multiple environmental disturbances on the pantograph-catenary interaction attracted increasing interests of many scholars. Song et al. [11] established the stochastic wind field along the railway catenary and investigated the wind-induced behaviour [12, 13], the aerodynamic instability [14] as well as the anti-wind strategies [15]. The vibration of vehicle excited by the irregular track surface was involved in investigating its effect on the pantograph-catenary interaction [16]. To improve simulation accuracy, the reattachment impact was included in the contact model of the pantograph-catenary [17]. The moving mesh methods [18, 19] were widely employed to improve simulation efficiency. The defects of catenary, including the tension loss [20], irregularities [21], variant height [22], defective droppers [23] and wear [24] were properly modelled, and their effects on the current collection quality were assessed.

Recently, double pantographs-catenary interaction performance has attracted the attention of several scholars. In [25], a methodology was proposed to predict the current collection quality of multiple pantographs-catenary. In [26], the wave propagation interference between the double pantographs was investigated, and a formula to calculate the optimal pantograph interval was proposed. Similar work was also conducted in [27], in which the formula for optimal pantograph interval was proposed based on the catenary mode shape. In [28], a more appropriate formula for double pantographs' interval was developed considering the variation of the catenary mode with different speeds. It can be seen that the previous research studies mainly focused on the optimisation of double pantograph interval with a certain catenary geometry and a given speed. This approach can only provide a theoretical optimal interval for double pantographs. In reality, the catenary is not a purely periodic structure. The span length, pre-sag and even the tension in the catenary always vary. The train speed cannot always be kept constant. All these realistic variations make it difficult to obtain an optimal interval for double pantographs.

Therefore, this article proposes another angle to improve the trailing pantograph performance. Some dampers can be placed in the catenary to reduce the intensity of the mechanical wave of the leading pantograph, and eliminate its effect on the trailing pantograph. In this work, the damper is added on the steady arm to absorb the vertical vibration energy. A mathematical model of double pantographs-catenary interaction is built to investigate the effect of the steady arm dampers on the current collection quality. Based on the simulation results, a group of realistic steady arm dampers is developed and its vibration suppression effect is validated through the experimental test.

2 | MODELLING OF DOUBLE PANTOGRAPHS-CATENARY

A mathematical model of the double pantographs-catenary system with steady arm damper is built. The catenary is modelled by the Absolute Nodal Coordinate Formulation (ANCF). An appropriate shape-finding procedure is presented to calculate the initial configuration of the catenary. The pantograph is assumed as a lumped-mass model. The validation of the present model is verified according to EN 50318 [29].

2.1 | Modelling of catenary by ANCF

The ANCF is a non-linear finite element method to adequately describe the element non-linearity when large deformation happens [30]. Figure 2 shows the catenary model based on the ANCF beam and cable elements. The ANCF beam element is utilised to model the messenger and contact wires. The tension and slackness of the dropper wire are modelled by the ANCF cable element. The steady arm is represented by the truss element without bending the degree of freedom (DOF). The clamps in the catenary are assumed as lumped masses. Here, the derivation of the stiffness matrix of the ANCF beam element is given as follows. The DOF vector that contains the displacements and the gradients for a beam element is defined by

$$\mathbf{e} = \left[x_i \quad y_i \quad z_i \quad \frac{\partial x_i}{\partial \chi} \quad \frac{\partial y_i}{\partial \chi} \quad \frac{\partial z_i}{\partial \chi} \quad x_j \quad y_j \quad z_j \quad \frac{\partial x_j}{\partial \chi} \quad \frac{\partial y_j}{\partial \chi} \quad \frac{\partial z_j}{\partial \chi} \right]^T \tag{1}$$

where, χ is the local coordinate in the undeformed configuration ranging from 0 to the element length L_0. The position vector in the deformed configuration $\mathbf{r}$ is interpolated by the shape function matrix $\mathbf{S}$ as

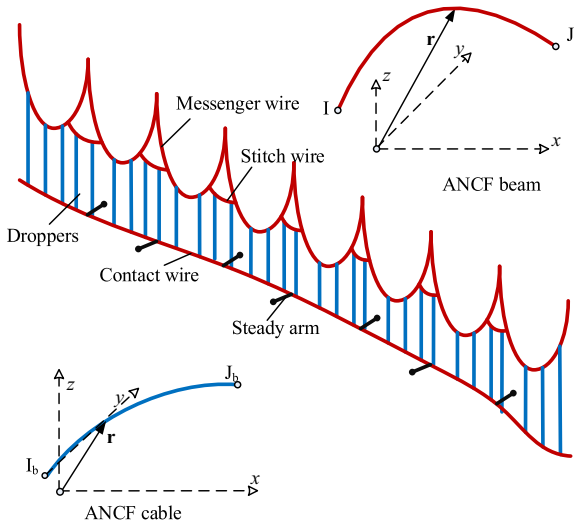

FIGURE 2 Catenary model based on ANCF beam and cable elements. ANCF, Absolute Nodal Coordinate Formulation

$$\mathbf{r} = \mathbf{S}\mathbf{e} \tag{2}$$

S is written by [31]

$$\mathbf{S} = \begin{bmatrix} S_1 & & S_2 & & S_3 & & S_4 & \\ & S_1 & & S_2 & & S_3 & & S_4 \\ & & S_1 & & S_2 & & S_3 & & S_4 \end{bmatrix}$$
$$S_1(\xi) = 1 - 3\xi^2 + 2\xi^3$$
$$S_2(\xi) = L_0\left(\xi + \xi^3 - 2\xi^2\right)$$
$$S_3(\xi) = 3\xi^2 - 2\xi^3$$
$$S_4(\xi) = L_0\left(\xi^3 - \xi^2\right) \tag{3}$$

in which, $\xi = x/L_0$. The strain energy obtained from the contribution of axial and bending deformation is expressed by [32].

$$U = \frac{1}{2}\int_0^{L_0}\left(EA\varepsilon_l^2 + EI\kappa^2\right)d\chi \tag{4}$$

in which E is Young's modulus, A is the section area, I is the moment inertial of the wire, ε_l is the longitudinal strain and κ is the curvature. The generalised elastic forces can be calculated by

$$\mathbf{Q} = \left(\frac{\partial U}{\partial \mathbf{e}}\right)^T = \mathbf{K}_e\mathbf{e} \tag{5}$$

The element stiffness matrix $\mathbf{K}_e$ can be defined according to Equation (5). In the shape-finding procedure, the tangent stiffness matrix is typically used to calculate the incremental nodal DOF vector $\Delta\mathbf{e}$ and the incremental unstrained length ΔL_0. The corresponding tangent stiffness matrices $\mathbf{K}_T$ and $\mathbf{K}_L$ with respect to $\Delta\mathbf{e}$ and ΔL_0 are derived as follows:

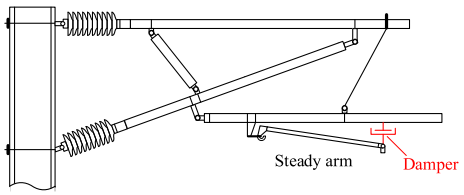

FIGURE 3 Configuration of the steady arm damper

$$\Delta\mathbf{F} = \frac{\partial\mathbf{Q}}{\partial\mathbf{e}}\Delta\mathbf{e} + \frac{\partial\mathbf{Q}}{\partial L_0}\Delta L_0 = \mathbf{K}_T\Delta\mathbf{e} + \mathbf{K}_L\Delta L_0 \tag{6}$$

Similarly, the tangent stiffness matrices of the ANCF cable element can also be obtained without bending DOFs. The cable element used to model dropper can only withstand tension but not compression. Assembling the element matrices yield the global incremental equilibrium equation for the whole catenary as follows:

$$\Delta\mathbf{F}^G = \mathbf{K}_T^G\Delta\mathbf{U}_C + \mathbf{K}_L^G\Delta\mathbf{L}_0 \tag{7}$$

where $\Delta\mathbf{F}^G$ is the global unbalanced force vector. $\mathbf{K}_T^G$ and $\mathbf{K}_L^G$ are the global stiffness matrices related to the incremental nodal displacement vector $\Delta\mathbf{U}_C$ and the incremental unstrained length vector $\Delta\mathbf{L}_0$, respectively. However, $\begin{bmatrix}\mathbf{K}_T^G & \mathbf{K}_L^G\end{bmatrix}$ is not a square matrix. The number of unknowns is more than the number of equations, which leads to uncertain solutions. Therefore, additional constraint conditions should be provided as follows to suppress undesired movements, according to the design specifications of the catenary.

- The vertical DOFs of the dropper point in the contact wire are restricted to describe the pre-sag.
- The longitudinal direction of each node is restricted to suppress the undesired movement.
- The tensions are applied to the endpoints of messenger and contact wires.

Introducing the above three types of constraints in Equation (7), the strained and unstrained lengths of all the elements can be calculated.

In this work, the steady arm damper included in the catenary is also modelled. According to Figure 3, the steady arm can rotate in a vertical direction. To avoid the lateral rotation caused by strong wind or temperature variance, a cable is usually added between the steady arm and the cantilever. In this work, we replace the cable with a damper, which not only provides damping to suppress the vertical vibration but also to fulfil all functions of the anti-wind cable.

2.2 | Modelling of pantograph-catenary interaction

The pantograph is modelled by a lumped mass model. A penalty function method is utilised to couple the two systems. The contact force f_c can be calculated by the relative penetration δ.

$$f_c = \begin{cases} k_s\delta & \text{if } \delta > 0 \\ 0 & \text{if } \delta \le 0 \end{cases} \tag{8}$$

in which, the penetration δ can be evaluated by

$$\delta = z_p - z_c \tag{9}$$

where, z_p, z_c and z_{ir} are the vertical displacements of the pantograph head, the contact wire and the irregularity. Using Equation (8), the equation of motion for the pantograph-catenary system is written as follows:

$$\mathbf{M}^G\ddot{\mathbf{U}}(t) + \mathbf{C}^G\dot{\mathbf{U}}(t) + \mathbf{K}^G(t)\mathbf{U}(t) = \mathbf{F}^G(t) \tag{10}$$

where, $\mathbf{M}^G$, $\mathbf{C}^G$ and $\mathbf{K}^G(t)$ are the mass, damping and stiffness matrices for the pantograph-catenary system, respectively. In this analysis, the mass matrix $\mathbf{M}^G$ is considered a consistent mass matrix, and the damping matrix is assumed as the Rayleigh damping form. The steady arm damper is added in the damping matrix. $\mathbf{F}^G(t)$ is the external force vector. A Newmark integration scheme is adopted to solve Equation (10). The stiffness matrix $\mathbf{K}^G(t)$ is updated according to the catenary deformation in each time step to fully describe the non-linearity of the messenger/contact wires and the slackness of droppers. In the following analysis, MATLAB is used to implement the simulation of pantograph-catenary interaction.

2.3 | Validation of the present model

The EN 50318 [29] released in 2018 is adopted to verify the accuracy and validation of the present pantograph-catenary interaction model. In this standard, a reference model of catenary with double pantographs is provided for the validation of the simulation tools. In this numerical validation, the train speeds are set to 275 and 320 km/h, and the double pantograph interval is 200 m. Table 1 presents a comparison of the results against the range of acceptance. It is seen that all the results are in the range of acceptance, which can demonstrate the validation and convincing accuracy of the present model for simulating double pantographs-catenary interaction. Apart from the validation with the standard, the accuracy of the present model has been verified by the filed test data [2] and the world benchmark [33] in the authors' previous works.

TABLE 1 Comparison of the present method with the standard

Speed	275			
	1		2	
Pantograph	Range	Result	Range	Result
F_m [N]	141.5–146.5	143.1	141.5–146.5	144.4
σ [N]	31.9–34.8	33.3	50.0–54.5	51.6
σ (0–5 Hz) [N]	26.4–28.9	27.2	41.2–45.4	42.8
σ (5–20 Hz) [N]	16.2–22.4	19.3	25.2–34.7	29.3
F_{max} [N]	211.9–244	222.9	241–290	260.4
F_{min} [N]	71–86	85.8	14–50	34.5
Speed	**320**			
	1		2	
Pantograph	Range	Result	Range	Result
F_m [N]	166.5–171.5	169.4	166.5–171.5	168.8
σ [N]	49.5–62.9	53.7	30.2–43.8	42.3
σ (0-5 Hz) [N]	38.7–44.4	40.1	14.3–23.3	19.0
σ (5-20 Hz) [N]	29.0–46.2	35.7	29.0–46.2	37.9
F_{max} [N]	295–343	295.0	252–317	269.5
F_{min} [N]	55–82	60.0	51–86	59.7

3 | ANALYSIS OF NUMERICAL RESULTS

The catenary parameters from a Chinese passenger special line (Hengyang to Liuzhou railway) are adopted here to perform the analysis. The main geometrical and material parameters are given in Table 2. Using the shape-finding approach presented in Section 2, the initial configuration of the catenary is obtained and presented in Figure 4. The pantograph parameters for this line are adopted from [22]. In the following analysis, the pantograph interval is selected as 200 m. The train speeds in the simulation are 250 and 275 km/h, which are the maximum speeds allowed for this line.

3.1 | Results without steady arm damper

The numerical simulations are performed without steady arm dampers. At 250 km/h, the resulting contact forces are presented in Figure 5a. According to EN 50367 [34], some statistics including the mean value, maximum value, minimum value, standard deviation, statistical maximum/minimum values of the contact force are of great importance to reflect the current collection quality, which is presented in Figure 5b. The results at 275 km/h are presented in Figure 6. It is seen that the contact force fluctuation of the trailing pantograph is more significant than that of the leading pantograph. With respect to the leading pantograph, the trailing pantograph has a bigger maximum contact force and smaller minimum contact

TABLE 2 Comparison of the present method with the standard

	Catenary Material Property
Contact wire	Line density: 1.084 kg/m; tension: 20 kN;
	Young's modulus: 120 kN/mm^2; Cross section; 150 mm^2
Messenger wire	Line density: 0.849 kg/m; tension: 15 kN;
	Young's modulus: 105 kN/mm^2; Cross section; 120 mm^2
Dropper	Line density: 0.09 kg/m; clamp mass; 128 g (on CW) 181 g (on MW)
	Tensile rigidity: 1000 kN/m
Steady arm	Line density: 2.39 kg/m
	Catenary geometrical property
Encumbrance:1.6 m; interval of droppers: 9 m; number of droppers: 6; Number of span: 18; length of span 55 m; Stagger value: 0.3 m; Steady arm length: 1.2 m;	

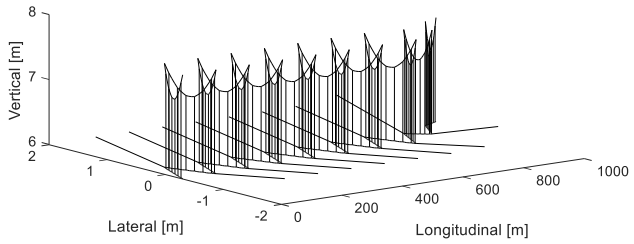

FIGURE 4 Initial configuration of the catenary

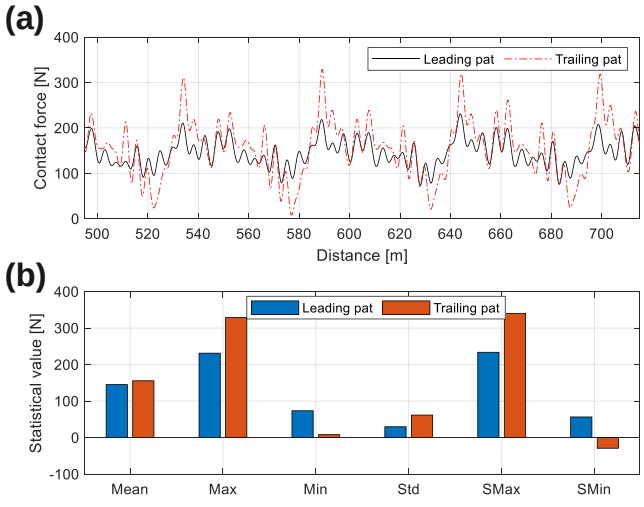

FIGURE 5 Simulation results of the contact force and statistical values at 250 km/h. (a) Contact force time-history, (b) Statistical values

force. The contact force standard deviation of the trailing pantograph is much larger than that of the leading pantograph. It should be noted that the statistical minimum contact force of the trailing pantograph is smaller than the acceptance threshold value 0 for the two speeds. Frequent arcing is expected to be observed for the trailing pantograph in reality.

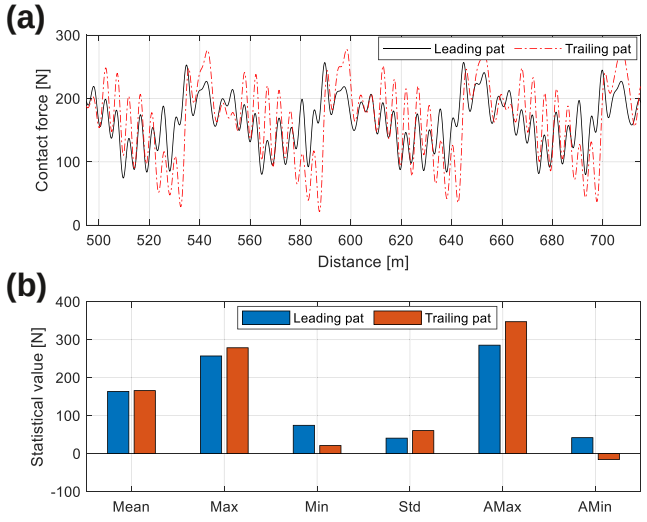

FIGURE 6 Simulation results of the contact force and statistical values at 275 km/h. (a) Contact force time-history, (b) Statistical values

3.2 | Results with the steady arm damper

The steady arm damping coefficient is selected from 0 to 600 Ns/m to evaluate its effect on the interaction performance. The resulting contact force standard deviations versus steady arm damping at 250 and 275 km/h are presented in Figure 7a,b, respectively. It is seen that the steady arm damping has the same effect on the leading pantograph at different speeds. However, for the trailing pantograph, its effect varies with different speeds. At 250 km/h, when the steady arm damping increases from 0 to 250 Ns/m, it causes the decrease of the contact force standard deviation of the trailing pantograph. When the steady arm damping increases over 250 Ns/m, the contact force standard deviation of the trailing pantograph undergoes a continuous growth. At 275 km/h, the contact force standard deviation of the trailing pantograph decreases with the steady arm damping coefficient increasing from 0 to 100 Ns/m, and increases when the steady arm damping is over 100 Ns/m.

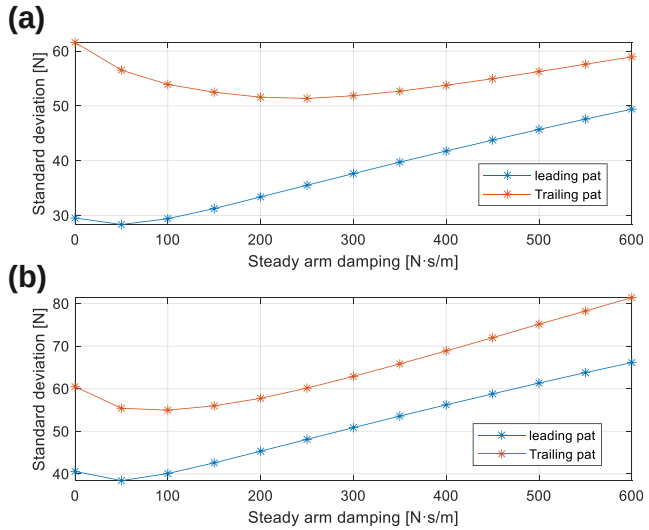

FIGURE 7 Simulation results of the contact force standard deviation versus steady arm damping. (a) at 250 km/h, (b) at 275km/h

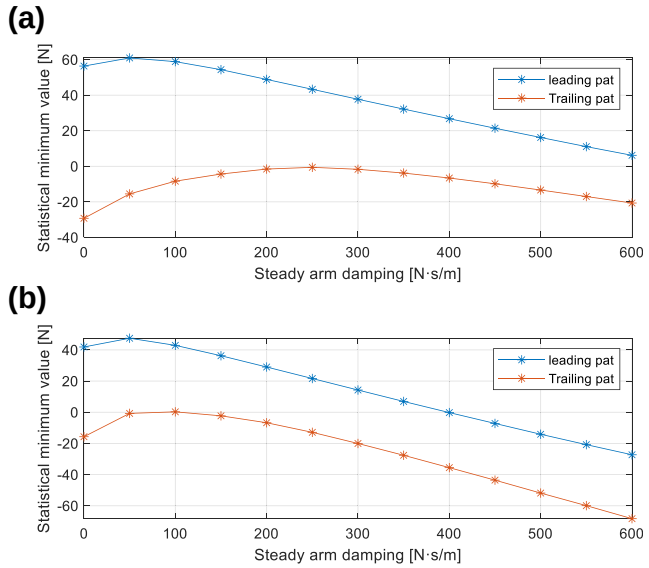

FIGURE 8 Statistical minimum contact force versus steady arm damping. (a) at 250 km/h, (b) at 275km/h

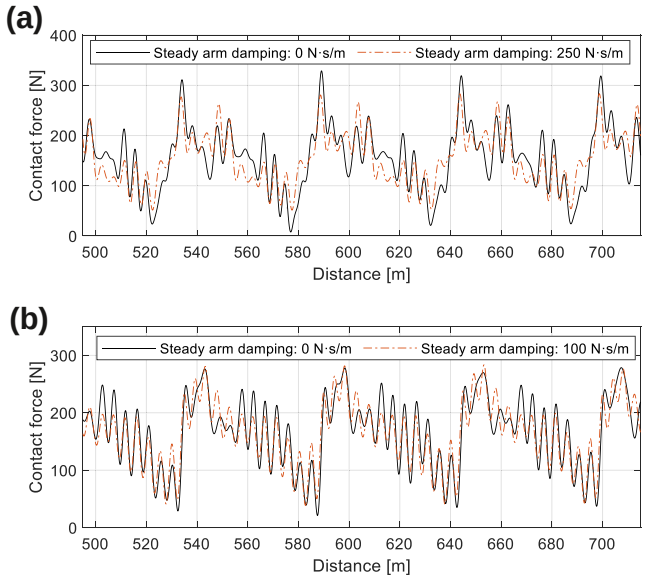

FIGURE 9 Contact force time histories. (a) at 250 km/h, (b) at 275km/h

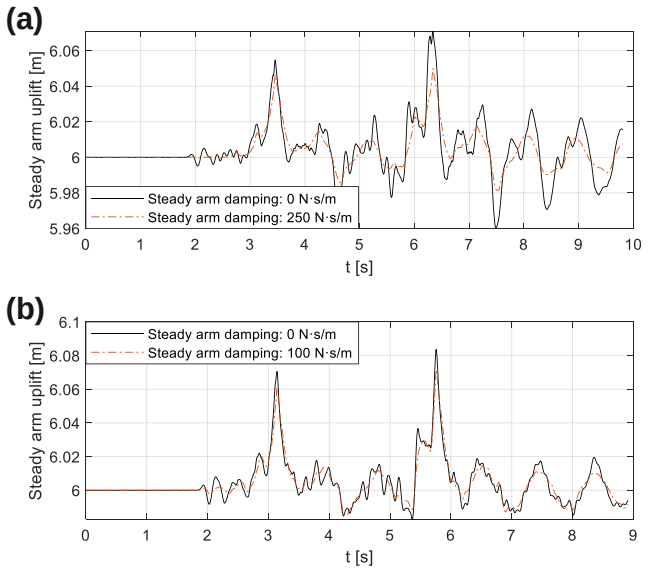

FIGURE 10 Steady arm uplift time histories. (a) at 250 km/h, (b) at 275km/h

The statistical minimum contact forces versus the steady arm damping at 250 and 275 km/h are presented in Figure 8a,b, respectively. It is seen that certain steady arm damping is effective to improve the minimum statistical contact force of the trailing pantograph. At 250 km/h, the steady arm damping of 250 Ns/m can lead to a positive statistical minimum contact force. Similarly at 275 Ns/m, the statistical minimum contact force increases to a positive value with the steady arm damping of 100 Ns/m. So it can be concluded that a certain steady arm damping can effectively improve the interaction performance of the trailing pantograph. For the given case, the best values of the steady arm damping are 250 and 100 Ns/m at the train speeds of 250 and 275 km/h.

The contact force time-histories with the best values of the steady arm damping are presented in Figure 9. When the steady arm damping is applied, the contact force at each speed shows a smaller fluctuation against the result without the steady arm damping. Notably, the minimum values of the contact force are increased by the presence of steady arm damping, which effectively lowers the possibility of arcing occurrence.

Apart from the contact force, the steady arm uplift is also an important index to evaluate the safety of the pantograph-catenary system. According to EN 50119 [35], maximum steady arm uplift should be restricted to avoid the damage of

the catenary caused by the pantograph impact. Figure 10a,b presents the steady arm uplift time-histories at 250 and 275 km/h, respectively. It is seen that the steady arm uplift is effectively restricted when the steady arm damper is included, which can reduce the possibility of the occurrence of wire breakage.

3.3 | Optimal damping values at different speeds

The above analysis demonstrates that the optimal value of the steady arm damping varies with different train speeds. In this section, the numerical simulations with different steady arm damping and train speeds are performed. The damping varies from 0 to 600 Ns/m with an interval of 50 Ns/m. The contact force standard deviations of the trailing pantograph are presented in Figure 11. Generally, the steady arm damper is effective when the damping is within 0–300 Ns/m. But the optimal value of steady arm damping is different at different speeds. At 200 km/h, the optimal steady arm damping is 100 Ns/m; At 225 km/h, the optimal value is 300 Ns/m; At 250 km/h, the optimal value is 250 Ns/m; At 275 km/h, the optimal value is 100 Ns/m; At 300 km/h, the optimal value is 50 Ns/m; At 325 km/h, the optimal value is 50 Ns/m.

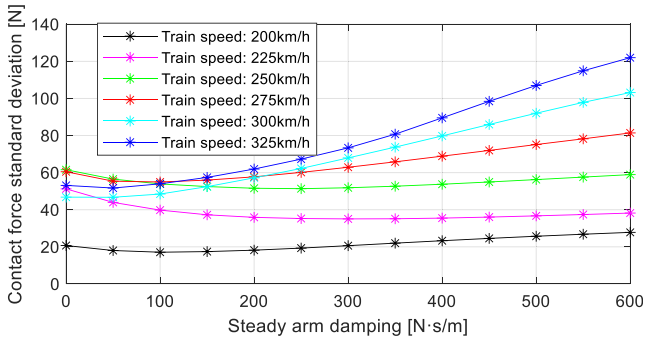

FIGURE 11 Contact force standard deviation of the trailing pantograph versus the steady arm damping at different speeds

4 | EXPERIMENTAL TEST

Through the above analysis, it is found that the best value of the steady arm damping varies with different train speeds. The appropriate values of the steady arm damping can be determined according to the normal operation speed of the network. The above analysis suggests that the optimal damping value varies from 100 to 300 Ns/m for the given case. In this section, the realistic steady arm damper is developed, and an experimental test is conducted to evaluate its capability to absorb the vibration of the contact wire.

4.1 | Development of the steady arm damper

As shown in Figure 12, the steady arm damper comprises a cylinder (2), a piston rod (3) and a piston (4). The right end is connected with the steady arm, and the left end is connected with the cantilever. When the contact wire moves upwards, the piston rod 3 and the piston 4 are driven to move to the left relative to the left end 6 and the cylinder 2. Thus, the working oil in the first working chamber A is squeezed and it flows through the damping groove 4-1 to the second working cavity B. The working oil generates damping during the flow process which acts on the piston 4 and reacts on the contact wire through the piston rod 3. In this way, the steady arm damper is able to reduce the vibration of the contact wire. The damping force f_d has the following relationship with the damping c_d

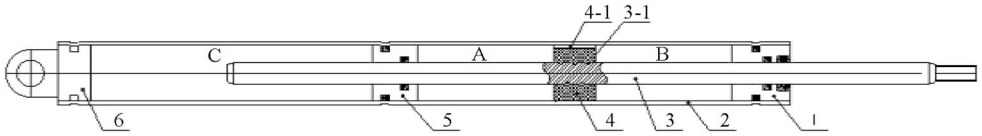

FIGURE 12 Steady arm damper

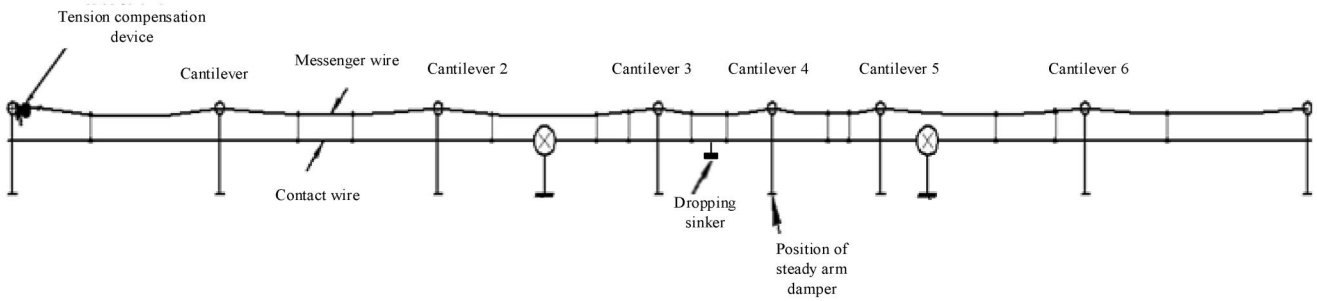

FIGURE 13 Schematics of catenary test bench

$$f_{\mathrm{d}} = c_{\mathrm{d}} v_{\mathrm{c}} \tag{11}$$

in which, v_{c} is the vertical speed of the contact wire. The damping c_{d} is relevant to the effective area of the damper, the shape and size of the cavity, and the viscosity of the working oil. Its value can be measured by experiment tests. According to the above analysis, three types of steady arm dampers are developed with the damping coefficients of 139.79, 189.76, 278.41 and 479.36 Ns/m.

4.2 | Experimental setup

The experimental test was conducted on the catenary test bench in China Railway Construction Electrification Bureau. The experimental setup is shown in Figure 13. The total length of the catenary is 74 m with six cantilevers. The wire is excited by a group of dropping sinkers with a mass of 10 kg. The sinker is attached to a certain point that is 5 m away from the steady arm damper, as indicated in Figure 13. As shown in Figure 14, the damper is installed on the steady arm which connects the contact wire and the cantilever. The displacement sensor is placed at the bottom of the steady arm damper to monitor the uplift of the contact wire. The displacement sensor is connected with the DH8303 dynamic signal test and analysis system. The sensor transmits the voltage signal to the dynamic signal testing and analysis system and converts it into the displacement waveform. Through the change of waveform generated by different dampers in the same position, the effect of different dampers with different damping coefficients on reducing the vibration amplitude of the contact wire can be evaluated.

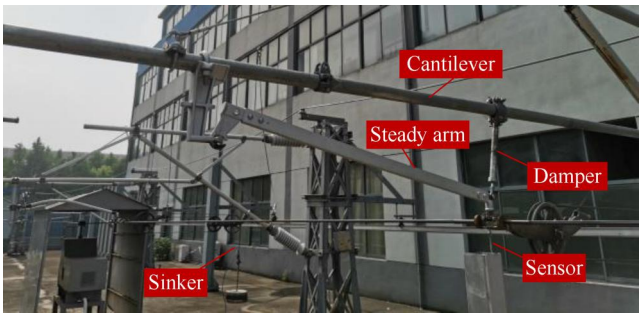

FIGURE 14 Experimental setup

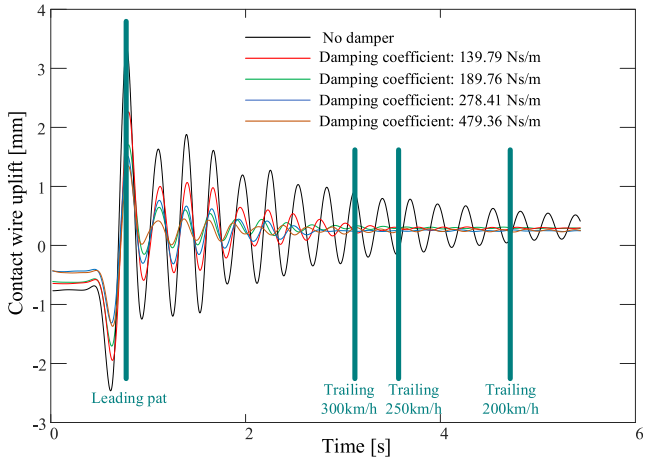

FIGURE 15 Contact wire uplift with different steady arm damping coefficients

4.3 | Experimental results

Figure 15 presents the measured contact wire uplift with different steady arm damping coefficients. It is seen that the increase of the steady arm damping coefficient can effectively reduce the wave intensity caused by the dropping sinker. The maximum uplift without damper reaches 3.47 mm. The steady arm dampers with 139.79, 189.76, 278.41 and 479.36 Ns/m reduce the maximum uplift to 2.23, 1.78, 1.51 and 1.31 mm, respectively. Assuming that the first uplift peak is caused by the leading pantograph, the time instants when the trailing pantograph reaches the measurement point with different speeds are denoted in Figure 15. It is seen that the steady arm damper can almost eliminate the contact wire vibration when the trailing pantograph passes. In this way, the effect of the mechanical wave on the trailing pantograph can be significantly reduced. However, the simulation results in Section 3.3 demonstrates that the current collection quality does not always improve with the increase of the steady arm damping coefficient. This may be caused by the hard spot introduced by the steady arm damper. When the pantograph passes, the steady arm damper disrupts the uplift of the pantograph head and results in excessive contact force. The moderate damping coefficient should be determined according to the design data of the catenary and the normal operating speed.

5 | CONCLUSIONS

When the double pantographs are used to collect current from the catenary, it is a common issue that the trailing pantograph is affected by the mechanical wave propagation excited by the leading pantograph. To improve the interaction performance of the trailing pantograph, a steady arm damper is developed in this article to reduce the wave intensity and its impact on the trailing pantograph. The non-linear model of catenary with the steady arm damper is modelled using ANCF. Through the numerical simulations with different damping coefficients and different speeds, the results show that the steady arm damper with certain values can reduce the contact force variation of the trailing pantograph. But overlarge damping may behave as a hard spot and aggravates the interaction performance. Generally, the steady arm damping should be not over 300 N s/m. The optimal value of the steady arm damping coefficient varies with the train speed. Thus, the steady arm damping should be determined according to the operating speed of a given line. Several realistic steady arm dampers are developed and placed on the catenary test bench. The experimental results demonstrate that the steady arm damper is able to absorb the mechanical wave generated by a dropping sinker.

In the future, the field test of the developed steady arm damper is desired to be performed before it can be used in the real line. The stress in the contact wire will be monitored to further investigate the performance of the steady arm damper.

ACKNOWLEDGEMENTS

This work was supported in part by the National Natural Science Foundation of China (U1734202; U51977182), and the Funding of Chengdu Guojia Electrical Engineering Co. Ltd (No. NEEC-2019-B09)

ORCID

Yang Song https://orcid.org/0000-0002-7699-5855

REFERENCES

1. Facchinetti, A., Mauri, M.: Hardware-in-the-loop overhead line emulator for active pantograph testing. IEEE Trans. Ind. Electron. 56(10), 4071–4078 (2009)
2. Song, Y., et al.: Wave propagation analysis in high-speed railway catenary system subjected to a moving pantograph. Appl. Math. Model. 59, 20–38 (2018)
3. Song, Y., et al.: Nonlinear modelling of high-speed catenary based on analytical expressions of cable and truss elements. Veh. Syst. Dyn. 53(10), 1455–1479(2015)
4. Cho, Y.H., et al.: Influence of contact wire pre-sag on the dynamics of pantograph-railway catenary. Int. J. Mech. Sci. 52(11), 1471–1490 (2010)
5. Kulkarni, S., Pappalardo, C.M., Shabana, A.A.: Pantograph/catenary contact formulations. J. Vib. Acoust. Trans. ASME. 139(1), 011010 (2017)
6. Finner, L., et al.: Programme for catenary-pantograph analysis, PrOSA statement of methods and validation according EN 50318. Veh Syst Dyn. 53(3), 305–313 (2015)
7. Zou, D., et al.: Experimental and simulation study of wave motion upon railway overhead wire systems. Proc. Inst. Mech. Eng.-Part F J. Rail Rapid Transit. 231(8), 934–944 (2017)
8. Zhang, J., Liu, W., Zhang, Z.: Sensitivity analysis and research on optimisation methods of design parameters of high-speed railway catenary. IET Electr. Syst. Transp. 9(3), 150–156 (2019)
9. Jian, Z., et al.: Simulation analysis of offline characteristics between pantograph and catenary. IET Electr. Syst. Transp. 7(3), 252–257 (2017)
10. Barmada, S., et al.: Arc detection in pantograph-catenary systems by the use of support vector machines-based classification. IET Electr. Syst. Transp. 4(2), 45–52 (2014)
11. Song, Y., et al.: Nonlinear analysis of wind-induced vibration of high-speed railway catenary and its influence on pantograph-catenary interaction. Veh. Syst. Dyn. 54(6), 723–747 (2016)
12. Song, Y., et al.: Study on wind-induced vibration behaviour of railway catenary in spatial stochastic wind field based on nonlinear finite element procedure. J. Vib. Acoust. Trans. ASME. 140(1), 011010 (2018)
13. Wang, Z., et al.: Random response analysis of axle-box bearing of a high-speed train excited by crosswinds and track irregularities. IEEE Trans. Veh. Technol. 68(11), 10607–10617 (2019)
14. Song, Y., et al.: Analysis of the galloping behaviour of an electrified railway overhead contact line using the non-linear finite element method. Proc. Inst. Mech. Eng.-Part F J. Rail Rapid Transit. 232(10), 2339–2352 (2018)
15. Song, Y., et al.: Active control of contact force for high-speed railway pantograph-catenary based on multi-body pantograph model. Mech. Mach. Theor. 115, 35–59 (2017)
16. Liu, N., et al.: Study of vehicle pantograph-catenary dynamic performance based on ADAMS. In: Proceedings of Chinese Control Conference (CCC), pp. 10150–10155. Chengdu, China (2016)
17. Chu, W., Song, Y.: Study on dynamic interaction of railway pantograph-catenary including reattachment momentum impact. Vibration. 3(1), 18–33 (2020)
18. Song, Y., et al.: Developed moving mesh method for high-speed railway pantograph-catenary interaction based on nonlinear finite element procedure. Int. J. Rail Transport. 7(3), 173–190 (2019)
19. Jimenez-Octavio, J.R., et al.: A moving mesh method to deal with cable structures subjected to moving loads and its application to the catenary-pantograph dynamic interaction. J. Sound Vib. 349, 216–229 (2015)
20. Vesali, F., et al.: Static form-finding of normal and defective catenaries based on the analytical exact solution of the tensile Euler-Bernoulli beam. Proc. Inst. Mech. Eng.-Part F J. Rail Rapid Transit. 233(7), 691–700 (2019)
21. Song, Y., et al.: Contact wire irregularity stochastics and effect on high-speed railway pantograph-catenary interactions. IEEE Trans. Instrum. Meas. 69(10), 8196–8206 (2020)
22. Song, Y., et al.: A methodology to study high-speed pantograph-catenary interaction with realistic contact wire irregularities. Mech. Mach. Theor. 152, 103940 (2020)
23. Song, Y., Liu, Z., Lu, X.: Dynamic performance of high-speed railway overhead contact line interacting with pantograph considering local dropper defect. IEEE Trans. Veh. Technol. 69(6), 5958–5967 (2020)
24. Wang, H., et al.: Analysis of the evolvement of contact wire wear irregularity in railway catenary based on historical data. Veh. Syst. Dyn. 56(8), 1207–1232 (2018)
25. Pombo, J., Ambrsio, J.: Multiple pantograph interaction with catenaries in high-speed trains. J. Comput. Nonlinear Dynam. 7(4), 041008 (2012)
26. Liu, Z., et al.: On the implementation of an auxiliary pantograph for speed increase on existing lines. Veh. Syst. Dyn. 54(8), 1077–1097 (2016)
27. Zhang, W., et al.: Pantograph and catenary system with double pantographs for high-speed trains at 350 km/h or higher. J. Mod. Transp. 19(1), 7–11 (2011)
28. Xu, Z., Song, Y., Liu, Z.: Effective measures to improve current collection quality for double pantographs and catenary based on wave propagation analysis. IEEE Trans. Veh. Technol. 69(6), 6299–6309 (2020)
29. European Committee for Electrotechnical Standardization EN 50318: Railway applications - Current collection systems - Validation of simulation of the dynamic interaction between pantograph and overhead contact line. European Standards (EN), Brussels (2018)
30. Shabana, A. A.: Definition of ANCF Finite Elements. J. Comput. Nonlinear Dynam. Definition of ANCF Finite Elements. Journal of Computational and Nonlinear Dynamics 10(5), (2015). https://doi.org/10.1115/1.4030369
31. Schwab, A.L., Meijaard, J.P.: Comparison of three-dimensional flexible beam elements for dynamic analysis: Classical finite element formulation and absolute nodal coordinate formulation. J. Comput. Nonlinear Dynam. 5(1), 1–10 (2010)
32. Sun, B., et al.: Dependence of hydrogen embrittlement mechanisms on microstructure-driven hydrogen distribution in medium Mn steels. Acta Materialia 183(15), 313–328 (2020). https://doi.org/10.1016/j.actamat.2019.11.029
33. Song, Y., Rønnquist, A., Navik, P.: Assessment of the high-frequency response in the railway pantograph-catenary interaction based on numerical simulation. IEEE Trans. Veh. Technol. 69(10), 10596–10605 (2020). https://doi.org/10.1109/tvt.2020.3015044
34. European Committee for Electrotechnical Standardization EN 50367: Railway applications — Current collection systems — Technical criteria for the interaction between pantograph and overhead line European Standards (EN), Brussels (2016)
35. European Committee for Electrotechnical Standardization EN 50119: Railway applications — Fixed installations — Electric traction overhead contact lines European Standards (EN), Brussels (2013)

How to cite this article: Chu, W., et al.: Development of steady arm damper for electrified railway overhead contact line with double pantographs based on numerical and experimental analysis. IET. Electr. Syst. Transp. 11(3), 269–277 (2021). https://doi.org/10.1049/els2.12024